CFD MODELLING OF WAVE-MANGROVE INTERACTION VIA RANS AND VARANS APPROACHES

David M. Kelly[1], Frederick Mann[1], Azin Lamei[1], Douglas Pender[1], Florian Bellafont[2], Hans Bihs[3], Widar Wang[3], Gaurav Savant[4]

This study evaluates two methodologies for representing mangrove structures in a numerical wave tank (NWT) within the framework of a CFD model. The work is phase 1 of a broader project aimed at enhancing mangrove parametrisation in 2D-horizontal (2DH) coastal area models for long wave simulations. The primary objective is to identify optimal approaches for representing added mass (inertia) and drag forces, characterized by the Morison equation coefficients C_D (drag) and C_M (added mass), based on mangrove properties and hydrodynamic conditions. Two modeling techniques, Direct Forcing (DF) Reynolds-Averaged Navier-Stokes (RANS) and Volume-Averaged RANS (VRANS), are employed, each incorporating distinct parametrisation methods for mangrove structures. Additionally, two mangrove parametrisation approaches identified in the literature are analyzed, highlighting their respective strengths and limitations. Comparative results from both modeling techniques and parametrisation methods are presented, alongside a case study simulating a surge scenario with a modified Husrin model to replicate an Ohira-type mangrove forest typical of Florida ecosystems..

Keywords: Mangroves; CFD; Direct Forcing, VRANS, Morison equation, Nature Based Solutions; Storm Surge; Tsunami

INTRODUCTION

This paper summarises the findings of using two distinct methodologies to represent mangrove structures in a numerical wave tank (NWT) within the framework of a CFD model. The work is the first phase of a larger project that aims to improve the parametrisation of mangroves in reduced-dimension, 2D-Horizontal (2DH), coastal area models; specifically, long wave models. The primary goal is to determine approaches to best parameterise the effects of both added mass (inertia) and drag forces, based on the properties of individual mangroves and the hydrodynamic conditions (i.e. water depths and velocities). These forces are typically represented via the drag and added mass coefficients in the Morison equation, i.e. C_D and C_M respectively. Here two modelling techniques are used to determine the drag and inertia effects induced by mangroves: Direct Forcing (DF) Reynolds Averaged Navier Stokes (RANS) and Volume-Averaged RANS (VRANS). Each approach utilises a different parametrisation method for the inclusion of the mangrove structures; these are discussed in more detail in the next section. As well as different modelling approaches there are different parametrisation of the mangroves themselves. Two primary mangrove parametrisation were identified from the literature both with their own strengths and weaknesses. These are discussed in more detail below. This paper is structured as follows: §1 discusses the two mangrove parametrisation approaches, §2 outlines the DF and VRANS modelling approaches that were employed with a brief discussion of the requisite turbulence closure. Next, §4 shows results obtained using both types of mangrove parametrisation and model type (i.e. DF of VRANS) these are compared with results from the literature. In §5 a surge type scenario is considered, the Husrin et al. (2012) model is modified so that it mimics an Ohira et al. (2013) type forest (which is better suited to Florida mangroves). Finally, conclusions are drawn.

MANGROVE PARAMETRISATION

Two distinct parametrisation methods were investigated to represent mangroves within both the DF and VRANS models, those of Husrin et al. (2012) and Ohira et al. (2013). Husrin et al. (2012) parameterised mangroves using staggered arrays of both rigid and flexible cylinders. Three physically realistic models of mangrove trunk-roots systems spanning several root densities were first created. For each realistic model, three parameterised models of varying frontal area and submerged root volume ratio were then constructed using cylinders of various heights and diameters. These were tested under steady flow conditions and the hydraulic forces acting on the models recorded using a force transducer. These forces were compared with the realistic models by Husrin et al. (2012) to determine the most representative parametrisation. In the present study, mangrove model A2 was selected based on its performance in parametrisation testing and

[1]JBA Consulting, Edinburgh, EH14 4AP, United Kingdom
[2]JBA Consulting, Skipton, BD23 3FD, United Kingdom
[3]Department of Civil and Environmental Engineering, NTNU, Norway
[4]CHL, U.S. Army Engineer Research and Development Center, Vicksburg, USA

its similarity to the *Rhizophora Sp.* mangroves found in Florida. Here, we take the same approach as Husrin et al. (2012) and focus on the rigid model excluding the canopy. Model A2 mangroves have been created as an STL model (Figure 1) using a Python script and then duplicated, and distributed in a staggered arrangement, to represent a mangrove forest.

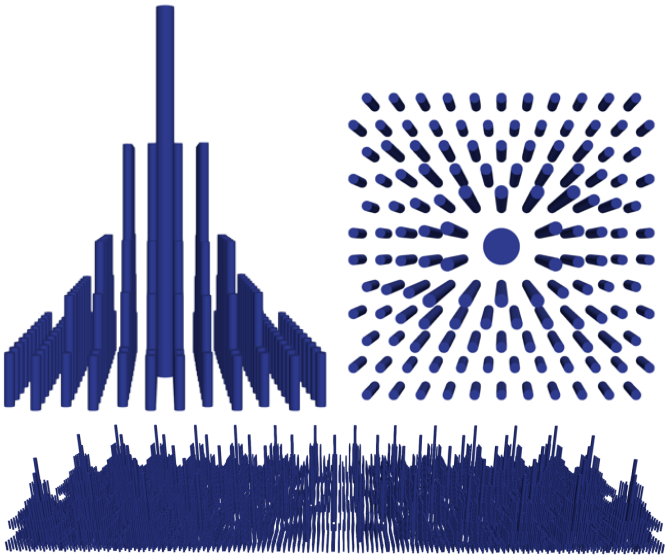

Figure 1: STL model of single mangrove and mangrove forest using the Husrin et al. (2012) parametrisation

The mangrove parametrisation of Ohira et al. (2013) has also been widely adopted in the literature (Maza et al. (2017), Shan et al. (2019), Maza et al. (2019), Tomiczek et al. (2020), Bryant et al. (2022), Kelty et al. (2022)). Ohira et al. (2013) used field measurements of Rhizophora mangroves to derive equations relating key parameters including the diameter at breast height (DBH), root height, number of roots and root diameter. This focused exclusively on the primary prop roots, assumed a quadratic root curvature and ignored the effects of the canopy. In the present study, the equations derived by Ohira et al. (2013) have been used to create an STL model of a single mangrove. This has then been duplicated to represent a mangrove forest (Figure 2).

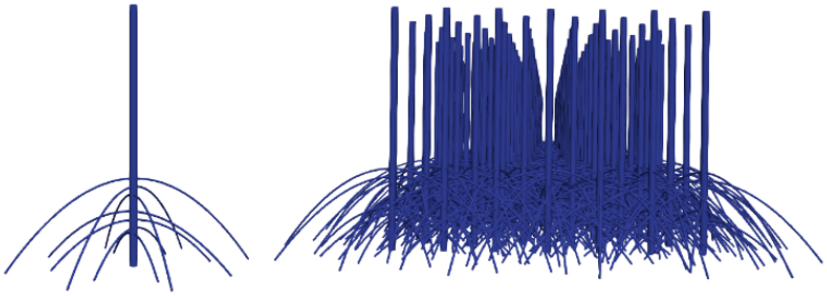

Figure 2: STL model of a single Ohira et al. (2013) mangrove (left) and a mangrove forest (right)

MODELLING APPROACHES

The DF model employs a microscopic approach, incorporating a detailed, geometrically representative model into the NWT. As no averaging is undertaken, other than the Reynolds averaging for turbulence, the pressure and velocity distribution around the model is determined locally. This allows for the derivation of key hydraulic relationships such as inertia and drag coefficients. These can be empirically related to non-dimensional parameters like the Reynolds (Re) and Keulegan Carpenter (KC) numbers to provide detailed information on the drag- and inertia-induced effects. The physical properties of the mangrove tree can be accounted for by the effective length, also referred to as an effective length scale/vegetation-related hydraulic

radius (L_e) in the literature, L_e is one of the available lengths that can be used to calculate Re alongside the DHB of the trunk and the root diameter. As opposed to the trunk diameter, which is constant, the effective length reflects the porosity of the root system that changes with the water depth. The value of L_e used in the Reynolds number expression can be derived from the frontal area and submerged volume of the mangroves. The representation of small, complex root structures is, however, computationally expensive and the accuracy of the solution is limited by this. As a result, the DF approach is typically used for simplified (parameterised) vegetation in a relatively small computational domain. The present study uses the DF approach to model the wave interaction with small-scale mangrove forests which are resolved on a tree-by-tree basis at the scale of individual roots and trunks. In the DF approach, the geometry of the mangroves is defined using stereolithography (STL) models, where a no-slip boundary condition is applied at the surface of the model. Wall roughness is used as the main tuning parameter to calibrate the model against experimental data and it is applied as a correction to the near-wall log-law velocity profile to increase turbulent dissipation (Nikuradse (1933)). Here, the equivalent sand grain roughness, k_s, is set to that for smooth cylinders (Husrin et al. (2012) used Teflon-coated tubes). Whilst there are approximate relationships for the equivalent sand grain roughness (Adams et al., 2012), within the DF framework k_s is a calibration parameter.

The VRANS model represents porous structures as a continuous medium, meaning that a detailed geometric description is not required (Higuera et al., 2014). The qualities of the porous structure are averaged over a computational cell. This macroscopic approach incorporates the drag- and inertia-induced (added mass) effects using pre-defined empirical coefficients based on the Reynolds number of the incoming flow and the characteristics of the porous media. The requisite empirical coefficients can only be determined through laboratory or numerical experiments. As such, the fundamental level of parametrisation in the DF approach cannot be achieved through VRANS. VRANS does, however, provide faster and computationally inexpensive solutions (relative to DF). Thus, VRANS studies are useful precursors to DF modelling. Moreover, a calibrated VRANS model is important as, due to its relative computational efficiency, it can be employed to validate a reduced dimension model (*i.e.* 2DH area model) for much more realistic scenarios than a DF model.

The governing equations of the VRANS numerical model are typically given in two formulations, *(i)* where the resistance forces by the porous material are provided as drag and inertia forces (Hur et al. (2008) and Maza et al. (2015)), and *(ii)* where the induced resistance force by the porous media is represented by the Forchheimer empirical equations (Hsu et al. (2002), Higuera et al. (2014) and Jensen et al. (2014)). Here, formulation *(i)*, namely the vegetation approach in REEF3D, is used to model mangroves. In this approach, the mangroves are represented as an array of vertical cylinders, which is more easily related to the morphological characteristics of a mangrove forest. Formulation *(i)* is defined assuming that the porous media represents an array of vertical, rigid cylinders (Maza et al. (2015)). This is a common approximation when modelling emergent vegetation. The governing equations of the VRANS model in which the vegetation resistance force, F_i, is modelled with drag and inertia forces are,

$$\frac{\partial \langle \bar{u}_i \rangle}{\partial x_i} = 0, \tag{1}$$

$$\frac{\partial \rho \langle \bar{u}_i \rangle}{\partial t} + \left\langle \bar{u}_j \right\rangle \frac{\partial \rho \langle \bar{u}_i \rangle \left\langle \bar{u}_j \right\rangle}{\partial x_j} - = -\frac{\partial \langle \bar{p} \rangle}{\partial x_i} + g_i x_j \frac{\partial p}{\partial x_j} + \frac{\partial}{\partial x_j} \mu \left(\frac{\partial \left\langle \bar{u}_j \right\rangle}{\partial x_j} + \frac{\partial \left\langle \bar{u}_j \right\rangle}{\partial x_i} \right) + F_i, \tag{2}$$

where ρ is the fluid density, $\langle \bar{u} \rangle$, $\langle \bar{\rho} \rangle$ and $\langle \bar{p} \rangle$ are the volume-averaged velocity, density and hydrodynamic pressure, respectively and F_i is

$$F_i = -F_{\mathrm{D}} - F_{\mathrm{I}}, \tag{3}$$

where F_{D} and F_{I} are the drag and inertia forces, respectively:

$$\bar{F}_{\mathrm{D},i} = \frac{1}{2} \langle \rho \rangle C_D D \, \mathrm{N} \langle \bar{u}_i \rangle \left| \langle \bar{u}_i \rangle \right|, \tag{4}$$

$$\bar{F}_{I,i} = \langle \rho \rangle C_M \frac{\pi D^2}{4} \, \mathrm{N} \frac{\partial \langle \bar{u}_i \rangle}{\partial t}, \tag{5}$$

where C_D is the drag coefficient, C_M is the inertia coefficient, D is the cylinder diameter and N is the number of cylinders per unit area. The four parameters controlling the drag and inertia forces are therefore

the product of C_D, N, D and C_M, N, D^2 respectively.
Two distinct calibration approaches were used for the Husrin et al. (2012) and Ohira et al. (2013) parametrisation. The Husrin et al. (2012) parametrisation consists of a single cylinder representing the trunk and several layers of cylinders, varying in height and density, representing the roots. This structure can be readily defined in REEF3D using several distinct vertical porous layers. Parameters C_D and C_M are initially based on values provided by Husrin et al. (2012), whilst N and D are based on the structural properties of the forest, which vary from layer to layer. To calibrate the model against the experimental results, C_D is then varied. The Ohira et al. (2013) parametrisation comprises a single cylinder representing the trunk and smaller, curved cylinders emanating from the trunk representing the roots. Here, the complexity of the root structures is not as easily represented by porous layers. As such, a single porous layer has been used to represent the entire mangrove forest. Within this layer, the average property is deemed to be suitably representative as to be meaningful. C_D, C_M, N and D are again initially based on values provided in the literature and the structural properties of the forest. To calibrate the model against the experimental results, N, a single free parameter shared by both K_D and K_I, is varied.

(DIS)ADVANTAGES OF THE TWO APPROACHES

The VRANS and DF approaches offer unique advantages and disadvantages when modelling mangroves and the two approaches can be used to complement each other. Table 1 summarises the benefits and drawbacks of each approach. The VRANS modelling can provide suitable set-ups for the more computationally demanding DF models. Once key input parameters have been found, using suitably calibrated DF models, the VRANS models can be employed to test the effects of forest length, hydrodynamic conditions etc, that are not feasible using DF models due to computational demand.

Table 1: Comparison of the key differences for the VRANS and DF methods

Aspect	VRANS Approach	Direct Forcing Method
Advantages	- Captures large-scale flow dynamics accurately - More computationally efficient for large domains - Suitable for complex flow regimes - Can be extended to investigate sediment transport around mangroves - Can be used to inform DF models - Can be used for ensemble experiments	- Directly accounts for vegetation-induced forces - Provides detailed local flow characteristics and forces - Can be more accurate for small-scale phenomena - Can yield C_D and C_M through numerical experiments - Allows for computation of actual frontal area and submerged volume
Disadvantages	- Requires empirical closure models for drag and added mass - Less detail on fine-scale interactions between flow and vegetation - Key quantities C_D and C_M required as input	- More computationally intensive - Less efficient for large scale or long-term simulations - Complexity/cost increases with root density - Complexity/cost increases with forest length - Limits the number of numerical experiments that can be undertaken

TURBULENCE CLOSURE SCHEME

Turbulent flows are described with a wide range of temporal and spatial scales. Modelling turbulent flow using direct numerical simulation (DNS) as a high-fidelity approach is extremely expensive and typically impractical. Therefore, a low-fidelity approach, RANS, is employed to empirically model the entire range of turbulent flow. The near-wall treatment in turbulence modelling is critical for accurately capturing the behaviour of the boundary layer, which directly influences flow separation and drag in the vicinity of a structure. In the present study, the $k-\omega$ turbulence model is used. This has a distinct advantage over the $k-\epsilon$ turbulence model as it integrates up to the wall without the need for additional wall or damping functions, which can introduce errors, especially in cases with complex near-wall phenomena like separation or strong pressure gradients. The ability to resolve the near-wall region makes the $k-\omega$ model particularly effective in predicting flow separation and reattachment, which are potentially important features of wave-mangrove interaction. Furthermore, in cases of flows over bluff bodies (*i.e.* mangrove roots and trunks), the model provides a more accurate representation of the wake dynamics by correctly modelling the near-wall and separated flow regions. However, $k-\omega$ shows limitations in non-turbulent regions away from walls. It assumes that regardless of the incoming flow conditions, the nature of the boundary layer between the wall and the outer region is the same. This may result in some inaccuracies with complex geometries. Furthermore, in the standard $k-\omega$ turbulence model, the dissipation rate ω is set to large values at the grid points adjacent to the solid wall. While this approach enhances the stability of the numerical model, it also makes the model sensitive to the near-wall grid spacing. Refer to Durbin (2017), Tomboulides et al. (2018)

and Xiao and Cinnella (2019) among others for a more detailed discussion on RANS and turbulence closure schemes.

EXAMPLE TEST CASES

Both the VRANS and DF models developed in the REEF3D NWT were validated against a wide range of different laboratory data from the literature. In this section we present results for some of the validation test cases that were run as part of this work. For brevity, descriptions of the laboratory set ups and hydrodynamic conditions simulated by the NWT are not provided here. The set-ups can be found by looking for the test name in the original references. The results presented provide realistic overview of the model ability to simulate the interaction of waves with complex mangrove structures; i.e. we have not cherry picked the best results. We present the results in two sections, those obtained using a Husrin type parametrisation and those obtained using an Ohira type parametrisation.

Husrin Model Cases

In this section we present some example results obtained for the solitary wave test cases described in Husrin et al. (2012) as well as the periodic wave cases described in the same paper. For the solitary wave cases, the models were run until the wave had propagated to the end of the domain. Time series comparisons were made between the numerical and experimental results at the gauges where experimental wave data was available (Figures 4, 5 and 6). They showed good agreement with an average absolute error (AAE) of 0.0069 m across all cases.

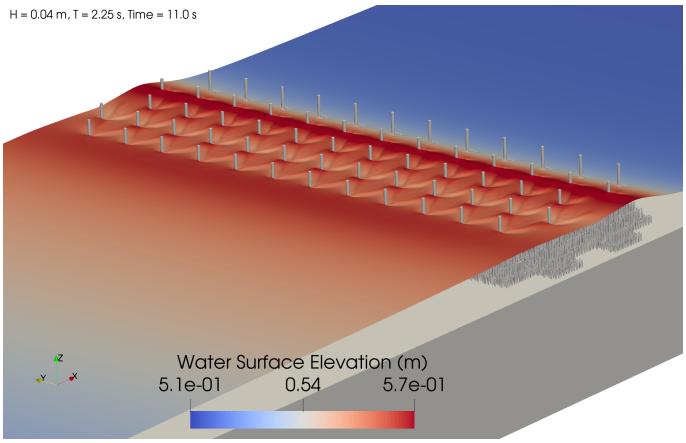

Figure 3: Water surface snapshot for the Husrin EM1_1 case simulated with the DF model

For EM1_1, whilst there was an additional bulking and a dispersive tail at WG10, this was rectified by the time the wave reached the start of the forest. Both the arrival time of the wave at the end gauge and the energy loss, both key quantities to inform the 2DH area modelling, are very well captured by the model. The EM2 case, which involved wave breaking and required a lower Courant number for stability, shows poorer agreement in wave amplitude and phasing compared to the EM1_1 and EM1_2 cases. This is likely due to the model not properly capturing the complex turbulence generation occurring from the combination of wave breaking and the wave-structure interaction. The model does, however, capture well the dissipation of energy caused by the forest as evidenced by the good quantitative agreement in wave height reduction. No time series data was available for the periodic wave cases.

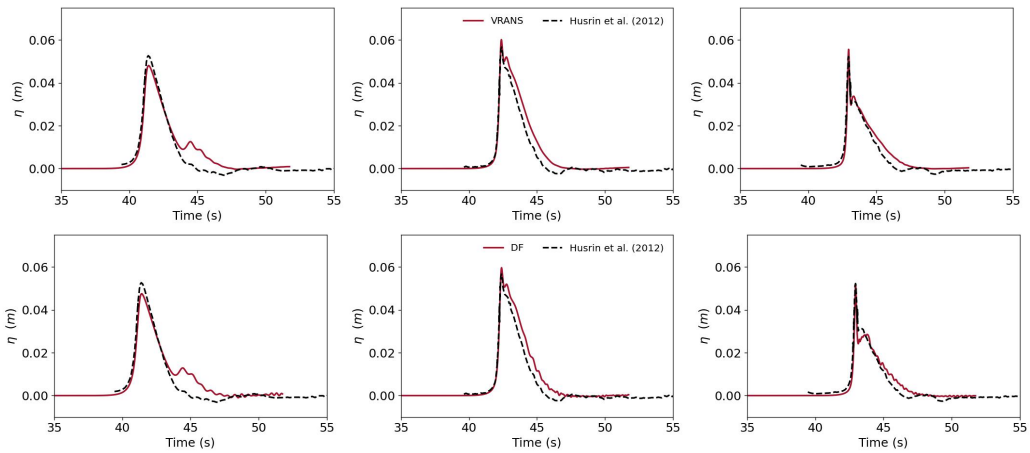

Figure 4: Surface elevation time-series for EM1_1 solitary wave case at gauges WG10, WG13 and WG14 respectively (left to right) VRANS results (Top) and DF results (Bottom).

Instead, comparisons have been made with K_t values (Table 3). The incoming wave height was averaged across WG5, WG6, WG7 and WG8 once the free surface had reached a quasi-steady state at around 40 seconds. Similarly, the transmitted wave height was averaged across WG18, WG19, WG20 and WG21.

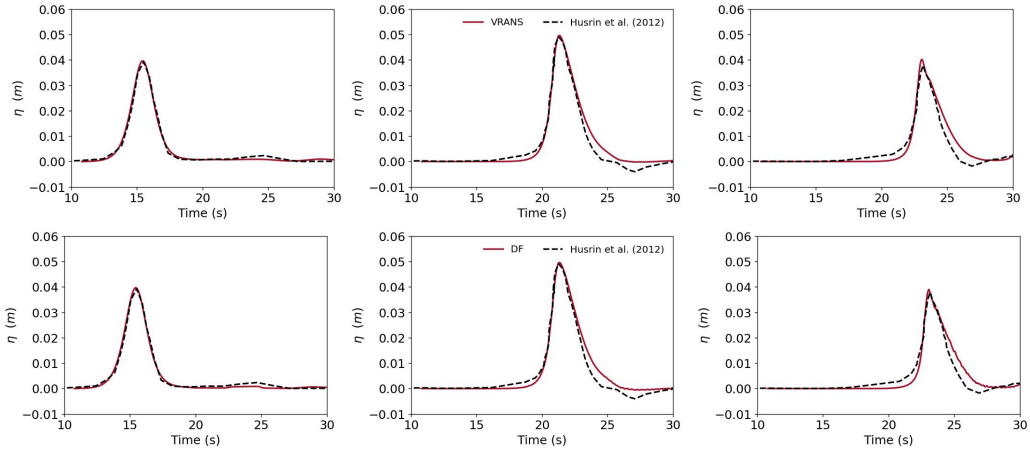

Figure 5: Surface elevation for EM1_2 solitary wave case at gauges WG5, WG13 and WG17 respectively (left to right). VRANS results (Top) and DF results (Bottom).

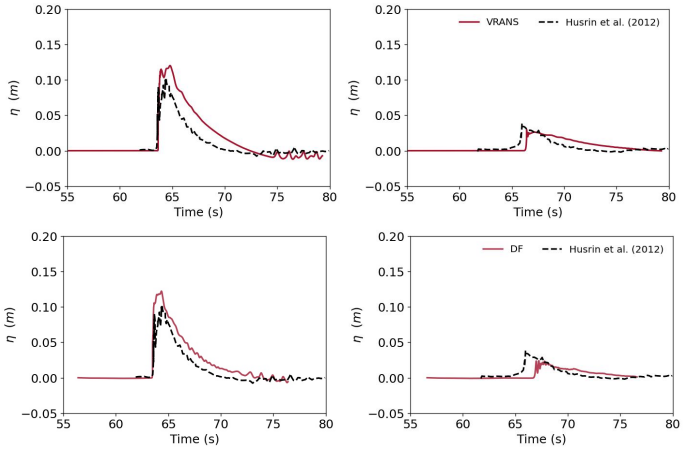

Figure 6: Surface elevation for the Husrin EM2 solitary wave case. VRANS results (Top) and DF results (Bottom) at gauges WG13 and WG17 respectively (left to right)

Table 2: Average absolute error for Husrin et al. (2012) VRANS solitary wave cases

Test case	AAE (m)	Average (m)
EM1_1	WG10: 0.004, WG13: 0.004, WG14: 0.003	0.0036
EM1_2	W5: 0.001, WG13: 0.002, WG17: 0.003	0.0020
EM2	WG13: 0.02, WG17: 0.01	0.0150
All cases	-	0.0069

Table 3: Transmission coefficients for the Husrin et al. (2012) regular wave cases

Test case	K_t (Measured)	K_t (VRANS)	Absolute error
reg1	0.560	0.573	0.013
reg2	0.195	0.285	0.090

Ohira–type Models

Initially, the Bryant et al. (2022) test case, which uses the Ohira parametrisation, was also considered for the calibration and validation of the DF model. It was found, however, that compared to the experimental results, the forest was overly dissipative. Despite repeated attempts at calibration, satisfactory results could not be obtained. It is believed that this is due to insufficient resolution of the smaller roots in the Ohira mangrove model. The large forest length and small root size also required large amounts of computational power compared with the relatively short forests presented in Husrin et al. (2012). This limited the number of calibration runs that could be attempted for this set-up. With this in mind, the focus was shifted to Husrin type forests to validate the model. It can be seen from the results presented above, the VRANS model performs well in simulating the wave energy attenuation in the Husrin cases. A separate VRANS model was also investigated for the Ohira type mangroves (as described in the modelling approaches section above) and good results were also obtained. We present results from two examples of simulations involving Ohira-type mangroves here.

Bryant et al. (2022) investigated the wave attenuation properties of a mangrove forest and the key parameters influencing this through near prototype scale (1:2.1) physical modelling. The VRANS model was run for

1200 seconds. Once the tank had reached a quasi-steady-state at around 50 seconds (Figure 7), the wave heights were averaged across the remaining duration and normalised against the incoming wave height at the start of the forest (Figure 8). Across all gauges, there was an AAE and MAE of 4.3% and 10.4%, with respect to the normalised VRANS results. This demonstrates good agreement between the numerical and experimental results. Although the local fluctuations along the forest were not captured, perhaps due to the limitations of the macroscopic approach in the VRANS model, the overall attenuation at the end of the forest was in good agreement.

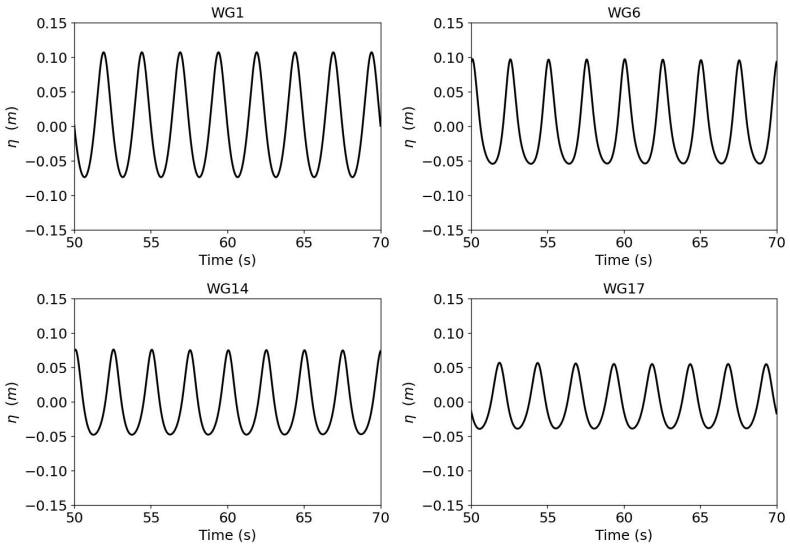

Figure 7: Surface elevation at various gauges in Bryant et al. (2022) VRANS model

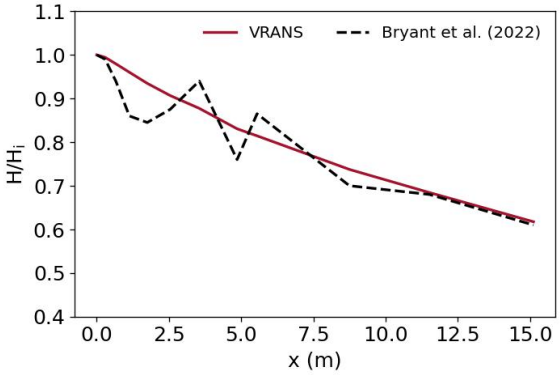

Figure 8: Wave damping as predicted by the VRANS model and as observed by Bryant et al. (2022) along the mangrove forest

Kelty et al. (2022) conducted prototype scale physical modelling to investigate the wave attenuation provided by mangrove forests. The study employed the parametrisation of Ohira et al. (2013) and placed the mangroves in a staggered arrangement to replicate a forest. Two forest set-ups were tested across a range of hydrodynamic conditions: a high-density case (0.75 trees/m^2) and a low-density case (0.375 trees/m^2). Water surface elevation, pressure and velocity were recorded for 100 seconds at intervals along the flume and used to calculate wave height decay and drag coefficient. The VRANS numerical model was run for 75 seconds to allow for comparison over the full experimental time series (Figure 9). The MAE and AAE at the peaks and troughs were calculated at each gauge once the free surface had reached a quasi-steady state at around 25 seconds. The average AAE at the peaks and troughs across all gauges was 0.008 m and 0.002 m respectively, demonstrating a good agreement between the experimental and numerical results.

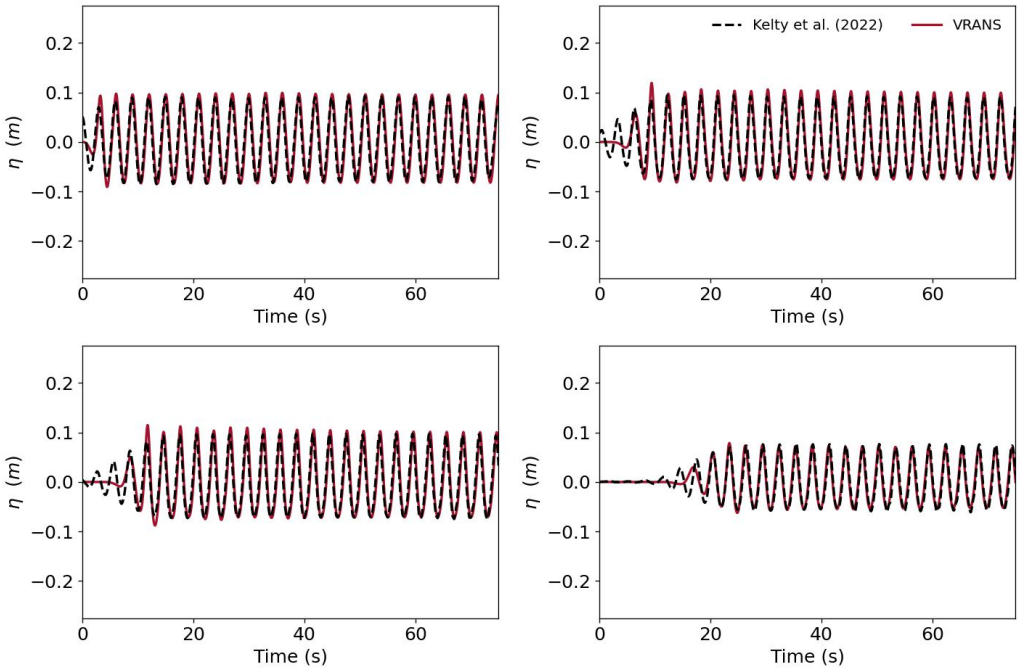

Figure 9: Surface elevation time series from the VRANS model and the Kelty et al. (2022) experiments. Clockwise from top left: WG1, WG2, WG12 and WG7.

Whilst the previous results have shown the ability of the VRANS model to capture the change in wave height, the final result presented here shows the ability of the model to correctly capture the depth-averaged (DA) velocity. Chang et al. (2022) present DA velocity results for periodic waves obtained at ADV1 in Figure 5 of their paper. It should also be noted that Chang et al. (2022) used 3D printed mangroves rather than an Ohira parametrisation.

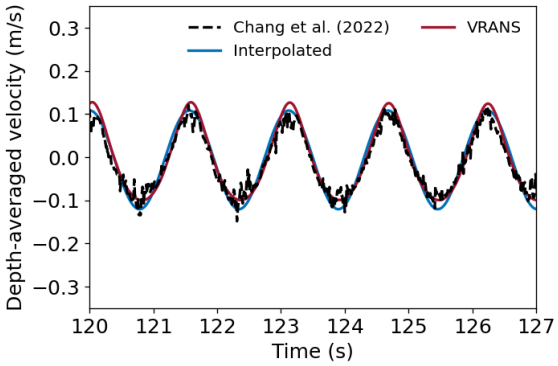

Figure 10: DA velocity time series for the VRANS model and Chang et al. (2022) experimental results.

Here we attempt to compare the DA model results with those presented in that figure. The VRANS model was run for 155 seconds to allow it to reach a quasi-steady state. The DA velocity was computed within the REEF3D model at ADV1 and plotted against time. This is compared to the raw experimental data and a best-fit line for this data in Figure 10. Good agreement is observed.

ACCURACY OF THE DF AND VRANS MODELS

The performance of several validation tests conducted using the REEF3D DF and VRANS models is summarised in Table 4.

Table 4: CFD NWT performance for VRANS and DF validation cases

Test case	Error metric	Error
Huang et al. (2011)	Average AAE (m)	0.002
Husrin et al. (2012) (VRANS)	Average AAE, all cases (m)	0.007
Chang et al. (2022)	Average AAE, peaks (m)	0.018
Kelty et al. (2022)	Average AAE, peaks (m)	0.008
Bryant et al. (2022)	AAE (% of REEF results)	4.3%
Husrin et al. (2012) (DF)	Average AAE, all cases (m)	0.007

STORM SURGE TYPE APPLICATION

Cases involving surge type conditions are lacking in the literature; most lab experiments employ either solitary or periodic waves. Using the calibrated and validated REEF3D DF RANS model, test cases were undertaken to investigate the interaction of a surge type wave with a mangrove forest. A turbulent bore resulting from wet-wet dam break initial conditions was employed to represent the surge. The submerged volume (V_m) and frontal area (A_f), from the Ohira model, over the water depth were used to create an equivalent Husrin-type mangrove model.

Table 5: Input conditions for the DF and VRANS surge model case LD_1

Test case	Bore Height (m)	Outflow (m^3/s)	Forest Density	Water Level (m)	Forest Length (m)
LD_1	1.0	51.75	Low	1.0	20.0

The roots are represented as vertical cylinders with the same diameter but varying heights, adjusted to get the correct V_m and A_f. Two cylinder diameters were used to create the Husrin-type mangrove model roots: 5cm, close to the Ohira root diameter and 10cm, corresponding to half the trunk diameter (as in the Husrin et al. (2012) A2 model). The submerged volume and frontal area over the water depth are shown in Figure 11. The different cylinders are strategically placed to avoid overlapping and provide the correct frontal area, i.e. no cylinder is hidden behind another. The model domain chosen extends 40 m in the x-axis, 12 m in the y-axis and 5 m in the z-axis, with the 20 m long forest at the centre (Figure 12). Nine gauges (G1-G9) are placed throughout the forest to record the free surface elevation and depth-averaged velocity. A force box is included around the central mangrove to record the time-varying force (Figure 13).

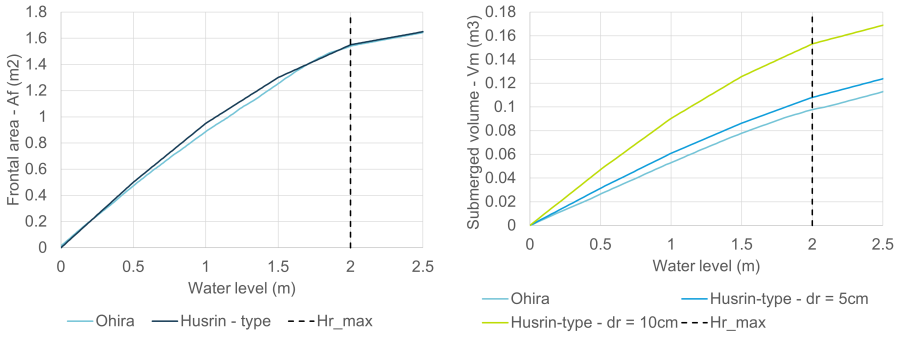

Figure 11: Frontal area (left) and submerged volume (right) over the water depth.

Results from the DF model were used to inform the values of C_D and C_M used in a VRANS model. The coefficients were obtained using computed forces and the Morison equation via the least squared fitting approach detailed in Chang et al. (2022). In line with Chang et al. (2022), the gauge directly in front of the central mangrove (G3) was used for the least squares fitting. The VRANS model was then used to run a larger range of hydrodynamic and mangrove configurations.

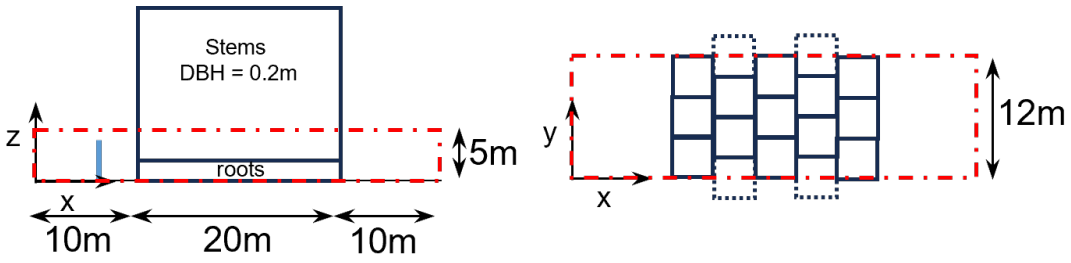

Figure 12: Dimensions of the numerical wave tank (NWT) for the direct forcing simulations: (dashed red lines) NWT extent, (blue line) maximum water level (4m), (dashed black lines) mangroves partially included due to the staggered tree configuration.

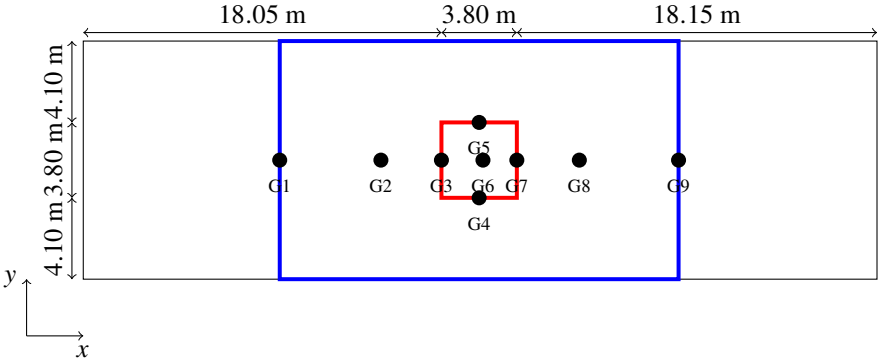

Figure 13: Domain for DF mangrove model with mangrove forest (blue), gauges (black) and force box (red)

As part of the initial analysis, results from the VRANS models were compared to corresponding DF models to cross-validate the calculated C_D and C_M values. Acceptable agreement is generally seen along the length of the forest for the free surface elevation. An example time-series comparison for the LD_1 experiment, with the set-up as detailed in Table 5, is shown in Figure 14.

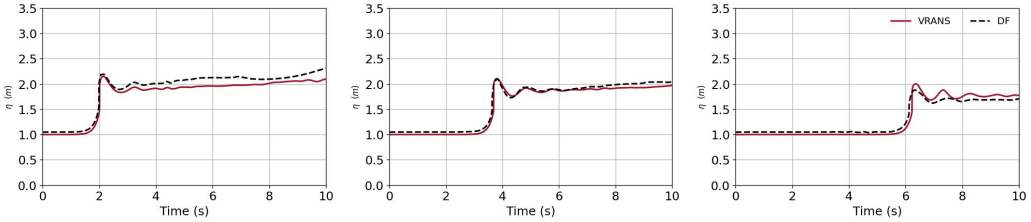

Figure 14: Comparison between the DF (black dashed) and VRANS (red solid) mangrove models for surge case LD_1 at (left to right) the start (G1), middle (G3) and end (G9) of the forest

CONCLUSION

This work forms part of the first phase on improving the parametrisation of mangroves in 2DH coastal area, long wave type, models. Based on the work undertaken, a subset of which is presented here, it can be concluded that VRANS modelling using the REEF3D model is capable of providing meaningful data with regards to wave height and energy dissipation by mangroves. Whilst DF models, based on REEF3D, offer great potential they are often too expensive computationally to provide results at forest scale. Such DF models can, however, be employed to inform VRANS models which can, in turn, be used to conduct a relatively large number of numerical experiments. These experiments, along with data in the literature, can be used to inform an improved 2DH coastal area model. We have parameterised mangroves with the characteristics found in Florida (height, root density etc.) within the Husrin–type mangrove framework. We

note that the Husrin mangroves have too high a root density compared to the mangroves typically found in South Florida. Specifically, the Ohira model (which is representative of both the mangrove species and characteristics found in Florida) is used to determine the correct behaviour of both frontal area $A_m = A_m(h)$ and submerged volume $V_m = V_m(h)$ with water depth $h = h(x, y, t)$. This behaviour can then be mimicked within the Husrin model framework. The single free parameter employed in the Ohira model is the diameter at breast height (DBH). The value of the DBH can be obtained from the tree height using the allometric relations given in Chen et al. (2021). Meaning that Florida mangroves can be readily translated into the Husrin model. There is a distinct lack of data on the interaction of surge type waves with mangroves in the literature. The approach of generating a turbulent bore with specific characteristics in a DF model can be used as a first approximation for surge type conditions. Additionally, it was shown that the drag and added mass coefficient determined from the DF model, using least squares fitting techniques, can be used in the VRANS and reasonable agreement between the two models is observed. Thus, a relatively large number of VRANS experiments can then be conducted to obtains the wave height and energy attenuation for different hydrodynamic conditions and forest configurations (involving multiple mangrove types).

ACKNOWLEDGEMENTS

This work was supported by the USACE under ERDC grant number W912HZ-23-2-0019.

References

T. M. Adams, C. Grant, and H. D. Watson. A simple algorithm to relate measured surface roughness to equivalent sand-grain roughness. 2012. URL `https://api.semanticscholar.org/CorpusID:1785401`.

M. Bryant, D. Bryant, L. Provost, N. Hurst, M. McHugh, A. Wargula, and T. Tomiczek. Wave attenuation of coastal mangroves at a near-prototype scale. Technical report, Engineer Research and Development Center (U.S.), 9 2022.

C. Chang, N. Mori, N. Tsuruta, K. Suzuki, and H. Yanagisawa. An experimental study of mangrove-induced resistance on water waves considering the impacts of typical rhizophora roots. *Journal of Geophysical Research: Oceans*, 127(6), June 2022.

Q. Chen, Y. Li, D. M. Kelly, K. Zhang, B. Zachry, and J. Rhome. Improved modeling of the role of mangroves in storm surge attenuation. *Estuarine, Coastal and Shelf Science*, 260, 2021.

P. A. Durbin. Some recent developments in turbulence closure modeling. *Annual Review of Fluid Mechanics Annu. Rev. Fluid Mech*, 50:77–103, 2017.

P. Higuera, J. L. Lara, and I. J. Losada. Three-dimensional interaction of waves and porous coastal structures using openfoam. part i: Formulation and validation. *Coastal Engineering*, 83:243–258, 1 2014. doi: 10.1016/j.coastaleng.2013.08.010.

T.-J. Hsu, T. Sakakiyama, and P. L.-F. Liu. A numerical model for wave motions and turbulence flows in front of a composite breakwater. *Coastal Engineering*, 46:25–50, 6 2002. doi: 10.1016/S0378-3839(02)00045-5.

Z. Huang, Y. Yao, S. Y. Sim, and Y. Yao. Interaction of solitary waves with emergent, rigid vegetation. *Ocean Engineering*, 38(10):1080–1088, 7 2011. doi: 10.1016/j.oceaneng.2011.03.003.

D. S. Hur, K. H. Lee, and G. S. Yeom. The phase difference effects on 3-d structure of wave pressure acting on a composite breakwater. *Ocean Engineering*, 35:1826–1841, 12 2008. doi: 10.1016/j.oceaneng.2008.08.019.

S. Husrin, A. StrusiÅ„ska, and H. Oumeraci. Experimental study on tsunami attenuation by mangrove forest. *Earth, Planets and Space*, 64(10):973–989, oct 2012. doi: 10.5047/eps.2011.11.008.

B. Jensen, N. G. Jacobsen, and E. D. Christensen. Investigations on the porous media equations and resistance coefficients for coastal structures. *Coastal Engineering*, 84:56–72, 2 2014. doi: 10.1016/j.coastaleng.2013.11.004.

K. Kelty, T. Tomiczek, D. T. Cox, P. Lomonaco, and W. Mitchell. Prototype–scale physical model of wave attenuation through a mangrove forest of moderate cross-shore thickness: LiDAR-based characterization and Reynolds scaling for engineering with nature. *Frontiers in Marine Science*, 8:1–18, 1 2022.

M. Maza, J. L. Lara, and I. J. Losada. Tsunami wave interaction with mangrove forests: A 3-D numerical approach. *Coastal Engineering*, 98:33–54, 4 2015. doi: 10.1016/j.coastaleng.2015.01.002.

M. Maza, K. Adler, D. Ramos, A. M. Garcia, and H. Nepf. Velocity and drag evolution from the leading edge of a model mangrove forest. *Journal of Geophysical Research: Oceans*, 122(11):9144–9159, 2017. doi: 10.1002/2017JC012945.

M. Maza, J. L. Lara, and I. J. Losada. Experimental analysis of wave attenuation and drag forces in a realistic fringe rhizophora mangrove forest. *Advances in Water Resources*, 131:103376, 9 2019.

J. Nikuradse. Laws of flow in rough pipes. *NACA Technical Memorandum*, (1292), 1933. URL `https://ntrs.nasa.gov/api/citations/19930093938/downloads/19930093938.pdf`.

W. Ohira, K. Honda, M. Nagai, and A. Ratanasuwan. Mangrove stilt root morphology modeling for estimating hydraulic drag in tsunami inundation simulation. *Trees*, 27(1):141–148, 2 2013. doi: 10.1007/s00468-012-0782-8.

Y. Shan, C. Liu, and H. Nepf. Comparison of drag and velocity in model mangrove forests with random and in-line tree distributions. *Journal of Hydrology*, 568:735–746, 1 2019.

A. Tomboulides, S. M. Aithal, P. F. Fischer, E. Merzari, A. V. Obabko, and D. R. Shaver. A novel numerical treatment of the near-wall regions in the k–ω class of RANS models. *International Journal of Heat and Fluid Flow*, 72:186–199, 8 2018.

T. Tomiczek, A. Wargula, P. Lomonaco, S. Goodwin, D. Cox, A. Kennedy, and P. Lynett. Physical model investigation of mid-scale mangrove effects on flow hydrodynamics and pressures and loads in the built environment. *Coastal Engineering*, 162:103791, 12 2020. doi: 10.1016/j.coastaleng.2020.103791.

H. Xiao and P. Cinnella. Quantification of model uncertainty in rans simulations: A review. *Progress in Aerospace Sciences*, 108:1–31, 7 2019.